Applied Catalysis B: Environmental 322 (2023) 122093

Contents lists available at ScienceDirect

Applied Catalysis B: Environmental

journal homepage: www.elsevier.com/locate/apcatb

Ligands-triggered evolution of catalytic intermediates during periodate activation via soluble Mn(II) for organic contaminants' abatement

Yingxu Gong, Jimin Shen, Yining Wu, Linlu Shen, Shengxin Zhao *, Yanchi Zhou, Yabin Li, Lei Cui, Jing Kang, Zhonglin Chen *

State Key Laboratory of Urban Water Resources and Environment, School of Environment, Harbin Institute of Technology, Harbin 150090, China

ARTICLE INFO

Keywords:
Emerging organic contaminants
Periodate activation
Soluble Mn^{II}
High-valent Mn^{V}-oxo intermediates
Non-radical oxidation

ABSTRACT

Homogenous catalysis technology could be flexibly combined with existing water treatment facilities, which presents broad applicational prospects and deserves systematic study. This work reinvestigated the periodate (IO_4^-, PI) activation process mediated by hydrated Mn^{II} ions and highlighted the critical involvement of the in-situ formed colloidal MnO_2 (Mn^{IV}). Mn^{II} ions were directly oxidized to colloidal Mn^{IV} in the Mn^{II}/PI system, and the nascent Mn^{IV} could in turn activate PI to form Mn^{IV}-PI* complex as the reactive oxidant. Besides, several kinds of ligands were introduced into the Mn^{II}/PI oxidation system to explore their influences. Nitrilotriacetic acid (NTA) outperformed other selected ligands and could significantly enhance PI activation to degrade organic contaminants, which could achieve a removal efficiency of ~99% within seconds. Interestingly, the presence of NTA completely altered the catalytic pathways rather than just accelerating the generation of reactive oxidants. Combining the results of sulfoxide-probe transformation tests and the ^{18}O isotope-tracer experiments, we proposed that the high-valent manganese-oxo (Mn^{V}-oxo) species was the dominant reactive oxidant generated in the Mn^{II}/NTA/PI system, and the metastable Mn^{III} complex was the precursor of the Mn^{V}-oxo species. Notably, maintaining the Mn^{II} high-spin d^5 center and stabilizing the in-situ formed Mn^{III} intermediates were the crucial premises for the evolution of the catalytic oxidation process triggered by functional ligands. This work clarified the critical involvement of functional ligands during PI activation via soluble Mn^{II} and might also inspire the designing of heterogeneous catalyst modification for the water treatment technology.

1. Introduction

A broad spectrum of emerging organic contaminants (EOCs) frequently detected in environmental waters has become one of the global issues of increasing concern [1]. Water treatment facilities were designed to be an essential barrier to preventing human beings from the threat of EOCs. Among various water purification techniques, advanced oxidation processes (AOPs) have been acknowledged as one of the most promising technologies for removing EOCs from water. Chemical oxidation can rapidly oxidize EOCs under the contribution of active transient intermediates, such as free radicals, high-valent transition metal species, and transition metal peroxy complex [2,3]. Free radicals (e.g., hydroxyl radicals ($^{\bullet}OH$) and sulfate radicals ($SO_4^{\bullet-}$)) are known to rapidly oxidize EOCs at nearly diffusion-controlled rates; however, there are still some obstacles to practical applications due to their low selectivity and short half-life. There appears to be a promising strategy to expand the applicational prospects of AOPs technologies; that is, the novel AOPs systems that could generate more selective and potent oxidants for achieving targeted electron transfer from organic pollutants toward the reactive oxidative species need to be exploited, to overcome the disturbance of complicated water matrix.

Manganese (Mn) is one of the redox-active transition metals ubiquitous in the environment, and the cycle of Mn valence has been widely recognized as the critical constituent for the natural mitigation of pollutants containing aniline and phenol moieties [4-7]. Researchers have realized that this natural redox process could be simulated or enhanced to exploit effective decontamination technologies [1,5]. For instance, permanganate (Mn^{VII}) has been widely studied and used to remove EOCs from water, especially focusing on the generation of reactive manganese species (RMnS) often attracted considerable concerns [1,8,9]. Origin of the powerful oxidation ability from Mn^{VII} was mainly due to the generation of complexed Mn^{III} and nascent manganese oxides (MnO_2) [10,

* Corresponding authors.
E-mail addresses: shengxin_zhao@163.com (S. Zhao), zhonglinchen@hit.edu.cn (Z. Chen).

https://doi.org/10.1016/j.apcatb.2022.122093
Received 16 August 2022; Received in revised form 17 October 2022; Accepted 21 October 2022
Available online 30 October 2022

11]. Mn^{III} species could be stabilized by soluble ligands and form Mn^{III}-ligands complex, which could act as both electron acceptor and donor to presenting redox ability in the AOPs systems [12,13]. Previous studies demonstrated that Mn^{III}-ligands complex could significantly contribute to the degradation of various EOCs, especially phenolic and aniline compounds [14-16]. With regards to MnO_2, the nascent colloid or flocculant MnO_2 could enhance the oxidation performance of Mn^{VII}, mainly through the following two mechanisms: (i) direct oxidation of EOCs by MnO_2, (ii) MnO_2 acts as a catalyst to enhance Mn^{VII} oxidation ability [17,18,8]. With the research further developing, several recent studies found that the combination of Mn^{VII} and bisulfite can lead to the rapid oxidation of EOCs [19–21], which might be attributed to the generation of strong oxidative high-valent manganese-oxo (Mn^{V}) intermediates; meanwhile, bisulfite combines both reduction and complexation abilities, which was capable to induce and stabilize the transient Mn^{V}-oxo intermediates during the reduction process of Mn^{VII}. Inspired by the proposed mechanism, we wondered if the reagents with the oxidation and complexation abilities can react with Mn^{II} ions and subsequently generate strong oxidative RMnS to degrade EOCs from water.

Periodate (IO_4^-, PI) is an ideal candidate oxidant, which possesses strong oxidative ability (+ 1.60 V) and could complex with high-valent metal-oxo species (e.g., Cu^{III}) [22,23]. Besides, AOPs based on PI activation have recently received increasing attention on the elimination of EOCs from water. Several methods have been applied to activate PI, such as freezing [24], UV [25], solar sunlight [26], hydroxylamine [27], alkali [28], single-atom-cobalt supported on graphene [29], and iron-based bimetallic nanoparticles [30]. However, AOPs technologies based on PI activation are often faced with the following two problems. First, the identification of reactive oxygen species (ROS) and the mechanistic insights into the redox process was still ambiguous. Besides, the toxic iodine products potentially generated from PI activation brought environmental risks. A recent report employed Fe^{II} ions to activate PI for the removal of organic pollutants from water, and the high-valent iron-oxo species (Fe^{IV}-oxo) was determined as the dominant reactive oxidant, and the non-toxic iodate (IO_3^-) was the only iodine product [30]. Therefore, we speculated that Mn^{II} ions could also activate PI to generate reactive oxidants for degrading EOCs from water. Additionally, previous studies proved that some appropriate ligands could coordinate with RMnS to enhance their oxidative ability [12,32]. Thus, it is of great interest to introduce ligands into the Mn^{II}/PI system to explore if the ligands could influence the oxidation performance.

Herein, we explored the efficacy of the Mn^{II}/PI system to remove some representative EOCs from water. Meanwhile, we chose nitrilotriacetic acid (NTA) as a functional ligand and investigated the performance of the Mn^{II}/NTA/PI oxidation system. According to previous studies, NTA possessed complexation ability for tuning the coordination circumstance of transition metals, which has been widely used to enhance Fenton-like systems due to its biodegradable feature [33-35]. Besides, the generation of reactive oxidants during the above oxidation processes was further confirmed and compared to unveil the critical involvement of the functional ligand. Last but not least, other ROS and iodine products potentially generated in both systems and the degradation intermediates of SMX were identified to present detailed insights into the redox processes.

2. Materials and methods

2.1. Chemicals and Materials

Potassium periodate (PI), potassium peroxymonosulfate (PMS, $KHSO_5{\cdot}0.5KHSO_4{\cdot}0.5\ K_2SO_4$), potassium peroxydisulfate (PDS), potassium permanganate (PM), $MnSO_4$, methyl phenyl sulfoxide (PMSO), methyl phenyl sulfone ($PMSO_2$), dimethyl sulfoxide (DMSO), 2,2,6,6-tetramethylpiperidine (TEMP), 5,5-dimethyl-1-pyrrolidine-N-oxide (DMPO), nitrilotriacetic acid (NTA), sulfamethoxazole (SMX), phenol (PN), bisphenol A (BPA), atrazine (ATZ), *p*-chlorophenol (*p*-CP), *p*-nitrophenol (*p*-NP), tert-butyl alcohol (TBA), deuterium oxide (D_2O), $H_2^{18}O$ (97% ^{18}O-enrichment), and superoxide dismutase (SOD, 20,000 U/mg) were all purchased from Macklin Biochemical Technology Co., Ltd. (Shanghai, P.R. China). All solutions were prepared with ultrapure water drawn from Millipore Milli-Q water system unless otherwise stated. All the above chemicals and reagents were used as received without any further purification.

2.2. Experimental procedures

Oxidation experiments were initiated by adding a given volume of PI stock solution (10 mM, freshly prepared) to the solution containing organic pollutants and Mn^{II} (ions or its complex) at desirable concentrations with magnetic stirring speed of 200 rpm. Samples were taken at different time intervals, and a 0.9 mL sample was immediately quenched by the mixture of 50 μL dimethyl sulfoxide (DMSO) and 50 μL ascorbic acid (0.25 M), and the quenched sample was filtrated through a 0.22 μm filter for further analysis. As confirmed by our preliminary experiments, the filters used to pre-treat samples in our work has negligible adsorption effect for the selected contaminants and probe compounds (data not shown). If buffer species were required, either 5 mM of acetate buffer or 5 mM of borate buffer was employed for pH 4.0 − 7.0 or 7.0 − 9.0, respectively, with pH adjusted to the pre-setting value using NaOH and H_2SO_4 in advance. Except for ^{18}O isotope-tracer experiments that were conducted in 5 mL of $H_2^{18}O$ (more details are available in **Text S1** in the Supporting Information), all other batch experiments were carried out open to the air in 150 mL conical flasks containing 100 mL of reaction solution at 18 ± 2 °C. All degradation experiments were performed at least in duplicates, and the average data are presented. The preparation methods of Mn^{III} (complex), Mn^{IV} (colloidal MnO_2), Mn^{VI}, and Mn^{VII} are shown in **Text S2**.

2.3. Analytical methods and characterization techniques

The residual concentration of organic compounds was analyzed by high-performance liquid chromatography (HPLC) (Agilent-1200, U.S.) combined with a UV detector, and the detection details are shown in Table S1. The analytical approaches for HOI, I_2, I_3^-, and PI are described in **Text S3**. Detection for singlet oxygen and free radicals using 2,2,6,6-tetramethylpiperidine (TEMP) and 5,5-dimethyl-1-pyrrolidine-N-oxide (DMPO) as trapping agents was performed by electron paramagnetic resonance spectrometer (EPR, EMX-8/2.7, BRUKER, Germany), and more details are listed in **Text S4**. $^{16}O/^{18}O$ isotope-labelled methyl phenyl sulfone ($PMSO_2$) and the degradation intermediates of SMX were identified by an ultrahigh-performance liquid chromatography quadrupole time-of-flight premier mass spectrometer (UPLC-Q-TOF MS/MS, Agilent 6545, USA), and corresponding information is available in **Text S1** and **Text S5**. The scanning of ultraviolet-visible (UV–vis) spectra was performed on a UV2550 (Shimadzu, Japan) spectrometer.

2.4. Theoretical calculation

Gaussian 16 W software was adopted to optimize the structure and calculate the wave functions of SMX. To obtain meaningful results, these calculations were completed with the polarizable continuity model (PCM) using the integral equation formalism model (IEFPCM) at B3LYP/6–31 G (d, p) level [36]. The data were processed and analysed by Multiwfn 3.8 (dev) software [37,38]. The electrostatic potential (ESP) on the molecular surface, highest occupied molecular orbit (HOMO)--lowest unoccupied molecular orbital (LUMO) and isosurface of the orbital weighted (OW) Fukui function (FF) and dual descriptor (DD) were drawn with VMD [39]. The ECOSAR (version 2.0) program was used to estimate the acute toxicity of SMX and its transformation products toward fish, daphnids, and green algae. The T.E.S.T. program (version 5.1.0.0) was applied to predict the Ames mutagenicity of SMX

and its transformation products through a consensus method.

3. Results and discussion

3.1. Degradation of EOCs in the Mn^{II}/PI and Mn^{II}/NTA/PI systems

Fig. 1 comparatively shows the degradation of several representative EOCs in the Mn^{II}/PI and Mn^{II}/NTA/PI systems, such as sulfamethoxazole (SMX), phenol (PN), *p*-chlorophenol (*p*-CP), bisphenol A (BPA), atrazine (ATZ), and *p*-nitrophenol (*p*-NP). The negligible influence of acetate sodium buffer on the degradation of PN (as a model EOCs) is presented in Fig. S1. The Mn^{II}/PI system could competently degrade SMX, PN, *p*-CP, and BPA, while the degradation of *p*-NP and ATZ was relatively sluggish. However, the presence of NTA significantly enhanced the activating ability of soluble Mn^{II} for PI, resulting in an ultrafast degradation of the selected EOCs. Remarkably, the degradation of SMX, PN, *p*-CP, BPA, and ATZ in the Mn^{II}/NTA/PI system was extraordinarily rapid, finished within seconds (the time interval of the first sample was 10 s). Regarding *p*-NP, most of the target pollutant (~80%) was degraded within 30 s. For comparisons, the removal efficiency of PN and *p*-NP in several other AOPs systems were investigated, including Fe^{II}/peroxymonosulfate (PMS), Fe^{II}/peroxydisulfate (PDS), Fe^{II}/PI, and permanganate (PM)/bisulfite (BS). We controlled the dosage of manganese and iron ions and surprisingly found that the Mn^{II}/NTA/PI system significantly outperformed the above Fe^{II}-based AOPs systems (Fig. S2). Besides, the removal efficiency of PN and *p*-NP was similar in both Mn^{II}/NTA/PI and PM/BS systems. Notably, the dosage of Mn^{II} was less than PM because PI was the final electron acceptor in the Mn^{II}/NTA/PI system, which means the Mn^{II}/NTA/PI system possessed less residual manganese than the PM/BS system.

3.2. Identification of high-valent Mn^{V}-oxo species in the Mn^{II}/NTA/PI system

To identify the reactive manganese intermediates potentially generated in both systems, we adopted methyl phenyl sulfoxide (PMSO) as a chemical probe because it has been proved that PMSO can be oxidized by high-valent metal-oxo species with the formation of corresponding sulfone product (methyl phenyl sulfone, $PMSO_2$) and followed stoichiometric relationship [20,40-45]. As shown in Fig. 2a, PMSO was rapidly transformed to $PMSO_2$ in the Mn^{II}/NTA/PI system. However, the attenuation rate of PMSO in the Mn^{II}/PI system was significantly slower, and no generation of the corresponding $PMSO_2$ was detected within 3 min. With the varied initial concentration of PMSO, the generation of $PMSO_2$ in the Mn^{II}/NTA/PI system followed a stoichiometric relationship, and the yields of $PMSO_2$ were ~95 % (Fig. 2b). Besides, though the Mn^{VI} and Mn^{VII} compounds could also oxidize PMSO to $PMSO_2$, their responses for the transformation rates of PMSO were far less than that of the Mn^{II}/NTA/PI system (Fig. S3). The above results indicated that the Mn^{V}-oxo species might be the dominant RMnS in the Mn^{II}/NTA/PI system.

Multiple oxidants could stoichiometrically oxidize sulfoxide to sulfone, so the identification of Mn^{V}-oxo species requires more deliberation. One of the most distinguishing features of the oxidation process dominated by high-valent metal-oxo species is the oxygen-atom-exchange (OAE) reaction with the H_2O molecule, which leads to the generation of ^{18}O isotope-labelled oxidation products [31,40,46]. To provide more convictive evidence for the generation of Mn^{V}-oxo species, we performed the oxidation of PMSO by the Mn^{II}/NTA/PI system in $H_2^{18}O$ matrix to examine if the OAE reaction occurred. The theoretically calculated *m/z* of non-isotope-labelled $PMSO_2$ (noted as $PMS^{16}O^{16}O$) and ^{18}O isotope-labelled $PMSO_2$ (noted as $PMS^{16}O^{18}O$) in positive electrospray ionization mode was 157.032 and 159.036, respectively. Firstly, we analyzed the $PMSO_2$ standard using an UPLC-Q-TOF-MS, and the extracted ion chromatogram (EIC) of $PMS^{16}O^{16}O$ and $PMS^{16}O^{18}O$ is presented in Fig. S4, and the retention time of $PMSO_2$ was 6.2 min. Applying the Mn^{II}/NTA/PI system to oxidize PMSO in the $H_2^{18}O$ matrix, two peaks with respect to $PMS^{16}O^{16}O$ and $PMS^{16}O^{18}O$ appeared in EIC at the same retention time (Fig. 2**c**). The relative abundance of $PMS^{16}O^{18}O$ was ~75 %. Meanwhile, a +2 shift of *m/z* originated from the isotope-labelled fragments of $PMS^{16}O^{16}O$ and $PMS^{16}O^{18}O$ with *m/z* of 157.0322 and 159.0362, respectively, was also observed in the mass

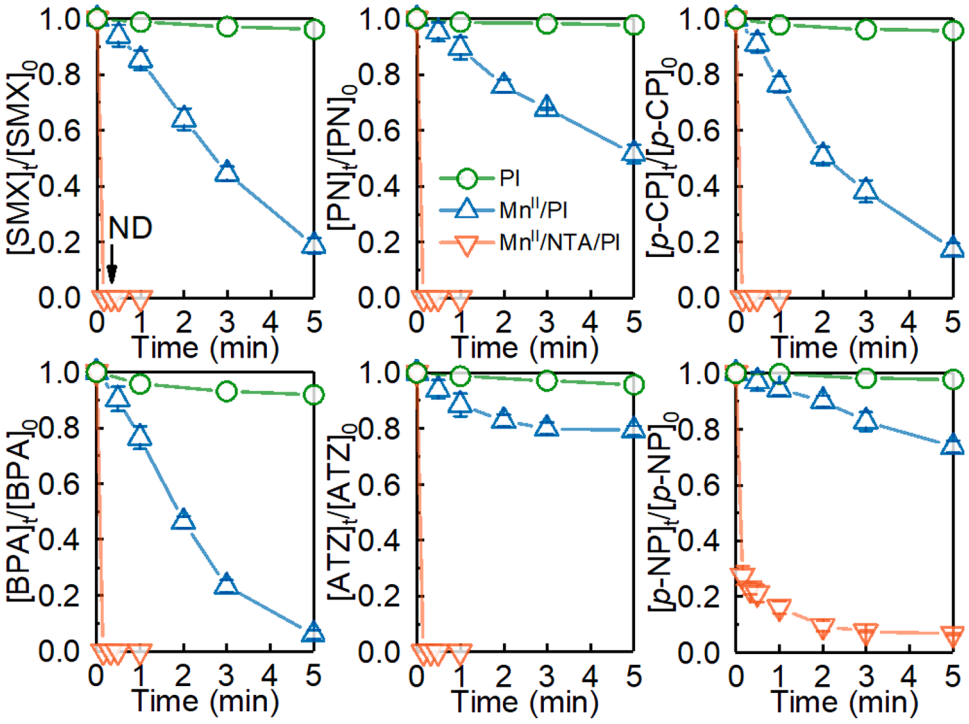

Fig. 1. Degradation of sulfamethoxazole (SMX), phenol (PN), *p*-chlorophenol (*p*-CP), bisphenol A (BPA), atrazine (ATZ), and *p*-nitrophenol (*p*-NP) in the Mn^{II}/PI and Mn^{II}/NTA/PI systems. Conditions: $[EOCs]_0$ = 10 μM, $[Mn^{II}]_0$ = 50 μM, $[NTA]_0$ = 250 μM, and $[PI]_0$ = 100 μM. pH = 5 (5 mM acetate sodium buffer).

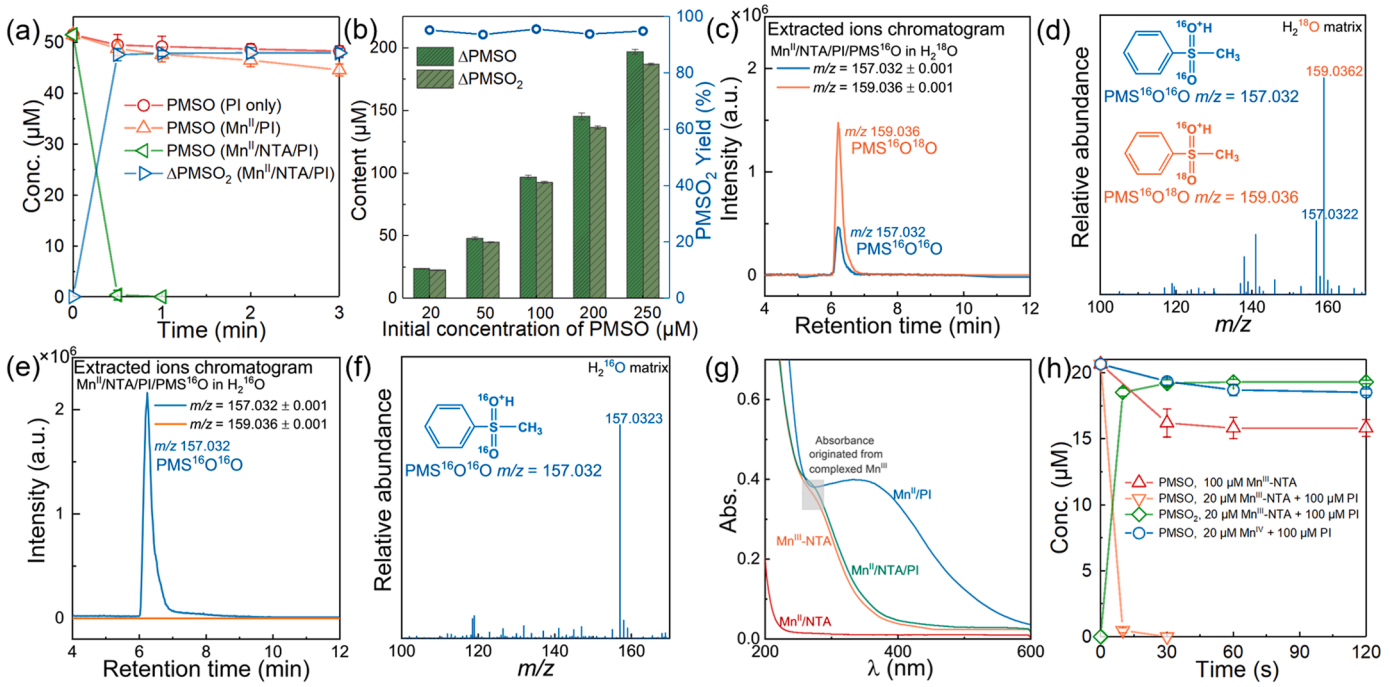

Fig. 2. (a) Consumption of PMSO in the alone PI, Mn^{II}/PI and Mn^{II}/NTA/PI systems, and the generation of PMSO$_2$ in the Mn^{II}/NTA/PI system. Conditions: $[PMSO]_0$ = 51.2 μM, $[Mn^{II}]_0$ = 50 μM, $[NTA]_0$ = 250 μM, and $[PI]_0$ = 200 μM. pH = 5 (5 mM acetate sodium buffer). (b) Consumption of PMSO and generation of PMSO$_2$ in the Mn^{II}/NTA/PI system with different initial concentrations of PMSO. Conditions: $[Mn^{II}]_0$ = 50 μM, $[NTA]_0$ = 250 μM, $[PI]_0$:$[PMSO]_0$ = 2:1 (mole ratio), pH = 5 (5 mM acetate sodium buffer), and Time = 3 min (c) Extracted ion chromatogram (EIC) of PMS^{16}O^{16}O (*m/z* = 157.032, $[M + H]^+$) and PMS^{16}O^{18}O (*m/z* = 159.036, $[M + H]^+$) generated during the oxidation of PMS^{16}O in the Mn^{II}/NTA/PI process in $H_2^{18}O$ matrix. (d) Corresponding MS analysis. (e) Extracted ion chromatogram (EIC) of PMS^{16}O^{16}O and PMS^{16}O^{18}O generated from the oxidation of PMS^{16}O in the Mn^{II}/NTA/PI process in $H_2^{16}O$ matrix. (f) Corresponding MS analysis. (g) UV–vis spectra for the mixture of Mn^{II}/NTA, Mn^{II}/PI, Mn^{II}/NTA/PI, and the prepared Mn^{III}-NTA complex solution. Conditions: $[Mn^{II}]_0$ = $[Mn^{III}\text{-NTA}]_0$ = 50 μM, $[NTA]_0$ = 250 μM, $[PI]_0$ = 100 μM, and Time = 2 min (h) Consumption of PMSO in the Mn^{III}-NTA/PI and Mn^{IV}/PI systems and the corresponding generation of PMSO$_2$ in the Mn^{III}-NTA/PI system. Conditions: $[PMSO]_0$ = 20.6 μM, pH = 5 (5 mM acetate sodium buffer).

spectra (Fig. 2d). In contrast, the relative abundance of PMS^{16}O^{18}O (*m/z* = 159.036) was negligible in the sample prepared in $H_2^{16}O$ matrix (Fig. 2e). Therefore, the above results collectively verified the successful incorporation of ^{18}O into the sulfone products during the sulfoxide oxidation, which could prove that the generation and contribution of high-valent Mn^{V}-oxo species in the Mn^{II}/NTA/PI system.

3.3. Critical involvement of the functional ligands

Another query warrants further study; that is, why the formation of Mn^{V}-oxo species was capable in the presence of NTA? Considering the strong complexation ability of NTA, we deduced that the presence of NTA was expected to stabilize the formed Mn^{III} intermediates, which might play an essential role during the generation of Mn^{V}-oxo species [32]. The critical role of Mn^{III} in manganese catalysis has been widely proposed, probably due to its d^4 ions in the $t_{2g}^3e_g^1$ state, and the electron in the antibonding orbital could be donated more favourable in the reaction [47-49]. To verify our hypothesis, we carried out the absorption spectra analysis of serial samples containing manganese in the UV and visible regions because it has been proved that complexed Mn^{III} under UV radiation could appear an absorbance peak (e.g., Mn^{III}-pyrophosphate has an absorbance peak at ~258 nm) [19]. As shown in Fig. 2g, a peak near 270 nm appeared in the absorption spectra of the Mn^{III}-NTA complex, and a similar absorption peak was also observed in the spectrum of Mn^{II}/NTA/PI, indicating that the in-situ formed Mn^{III} intermediates were coordinated and stabilized by NTA during PI activation. In addition, we found that the prepared Mn^{III}-NTA complex could also trigger PI activation and result in the rapid oxidation of PMSO with the stoichiometric generation of PMSO$_2$ (Fig. 2h). However, only ~25 % PMSO was oxidized by Mn^{III}-NTA alone within 2 min, and the oxidation of PMSO in Mn^{IV}/PI system was also not significant when compared with the Mn^{III}-NTA/PI system (Fig. 2h). Thus, we confirmed that the Mn^{III} complex was the critical metastable precursor of the Mn^{V}-oxo species, and that could explain the essential involvement of NTA during PI activation mediated by complexed Mn^{II}. Moreover, high-valent Mn-oxo species could be generated from low-valent Mn ions (or complex) through two-electron transfer (i.e., oxygen-atom-transfer) process. Therefore, the possible generation pathways of high-valent Mn-oxo species could be inferred as: Mn^{II}→Mn^{IV}, Mn^{III}→Mn^{V}, or Mn^{IV}→Mn^{VI}, so the above results also provided evidence to prove the valence of the RMnS should be Mn^{V}. To sum up, Mn^{II} was firstly oxidized to Mn^{III} by PI through one-electron transfer. The presence of NTA could capture and stabilize Mn^{III} intermediates through coordination, then the stabilized Mn^{III}-NTA complex could undergo further oxidation by PI via two-electron transfer along with the generation of Mn^{V}-oxo species as the critical RMnS, which contributed to the rapid degradation of EOCs from water.

Furthermore, we introduced other several different ligands into PI activation mediated by soluble Mn^{II} for SMX degradation, such as ethylenediamine tetraacetate (EDTA), pyrophosphate (PP), oxalate acid (OXA), and picolinic acid (PICA). As shown in Fig. 3a, EDTA and PP inhibited SMX degradation in the Mn^{II}/Ligand/PI system, but OXA and PICA exhibited promotion. We performed EPR analysis of the serial soluble Mn^{II} in the absence and presence of different ligands to obtain more information of the unpaired electrons in the Mn 3*d* subshell, and the results are shown in Fig. 3b. Mn^{II} hydrated ions presented a six-line hyperfine splitting signal near g = 2.005, which could be attributed to the high-spin d^5 center. In the presence of different ligands, the EPR signals were decreased or disappeared, indicating that the electrons in Mn 3*d* subshell were rearranged under the influence of the complexation. Interestingly, Mn^{II}-NTA, Mn^{II}-OXA, and Mn^{II}-PICA presented the six-line hyperfine splitting signals, and all these three kinds of ligands

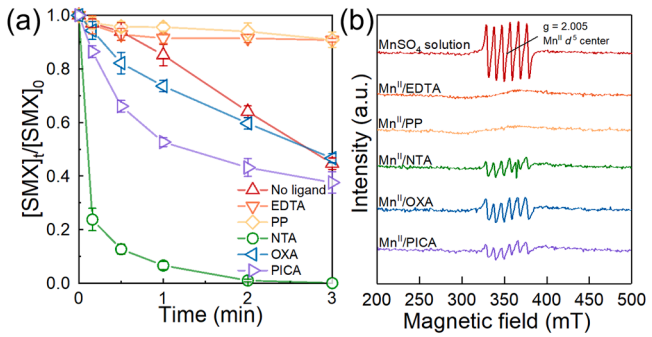

Fig. 3. (a) Degradation of SMX during PI activation via soluble Mn^{II} in the presence of different ligands, including ethylenediamine tetraacetate (EDTA), pyrophosphate (PP), oxalate acid (OXA), and picolinic acid (PICA). Conditions: $[SMX]_0 = 10$ μM, $[Mn^{II}]_0 = 50$ μM, $[ligand]_0 = 100$ μM, $[PI]_0 = 100$ μM, and pH = 5 (5 mM acetate sodium buffer). (b) EPR analysis of soluble Mn^{II} in the absence and presence of different ligands. Conditions: $[Mn^{II}] = 1$ mM, [Ligands] = 6 mM, and pH 5 (acetate buffer). A center field of 3500 G, microwave power of 50 mW, microwave frequency of 9.86 GHz, modulation frequency of 100 kHz, modulation amplitude of 1.0 G, conversion time of 40 ms, and sweep time of 40 s.

exhibited promotion performance during PI activation (Fig. 3a). Thus, except for stabilizing the nascent Mn^{III} intermediates, we speculated that the functional ligands should also maintain the high-spin d^5 center of Mn^{II} complex, which was capable to further undergo valence-shift to generate high-valent Mn^{V}-oxo species.

3.4. Transformation of PI in the Mn^{II}/NTA/PI System

It is of great importance to clarify the fate of PI after going through the one-electron transfer pathway during the generation of Mn^{III} species. Previous studies implied that multiple ROS could generate from PI activation mediated by UV [25], solar sunlight [26], alkaline [28], and hydroxylamine [27], such as $O(^3P)$, singlet oxygen ($^1O_2$), $^{\bullet}OH$, and superoxide radicals ($^{\bullet}O_2^-$). The free radicals and $^1O_2$ potentially generated in the Mn^{II}/NTA/PI system were trapped and tested by electron spin resonance (ESR) detection. As shown in Fig. 4a, we adopted DMPO as a trapper reagent to capture the potentially generated ROS; however, the signal of products presented heptad-peaks with an intensity ratio of 1:2:1:2:1:2:1 could be attributed to 5-dimethyl-1-pyrrolidone-N-oxyl (DMPOX), which was commonly ascribed to direct oxidation rather than a radical attack on DMPO [50-53]. According to previous studies, detection of superoxide radicals was carried out in methanol matrix to screen the interference of $^{\bullet}OH$ as well as to extend the lifetime of $^{\bullet}O_2^-$ [54,55]. However, the obtained characteristic signal was originated from DMPO-OCH_3 rather than DMPO-O_2^- (Fig. 4b), and the methyl oxygen radical ($^{\bullet}OCH_3$) might generate from the oxidation of methanol by Mn^{V}-oxo species. Besides, we used TEMP as the trapping agent to determine whether $^1O_2$ was generated in the Mn^{II}/NTA/PI system, and the result was negative (Fig. 4c). Thus, we attempted to perform the trapping experiments to capture $^1O_2$ in the D_2O matrix instead of H_2O due to the extended lifetime of $^1O_2$ up to 10 times in D_2O [56,57]. As shown in Fig. 4c, a faint signal of TEMPO was detected, indicating the possible generation of $^1O_2$ in the Mn^{II}/NTA/PI system. However, we deduced that the singlet oxygen could not be the dominant reactive oxidant in the Mn^{II}/NTA/PI system because SMX is inert toward $^1O_2$ [2, 58-60], which contradicts the rapid degradation of SMX in the Mn^{II}/NTA/PI system (Fig. 1).

In addition, quenching experiments were carried out to further identify the contribution of the potential generated ROS to SMX degradation (Fig. 4d). We found that *tert*-butyl alcohol (TBA) presented negligible effects on the degradation of SMX, which could exclude the contribution of $^{\bullet}OH$. Besides, the degradation of SMX was significantly inhibited by the coexisted dimethyl sulfoxide (DMSO), which could be

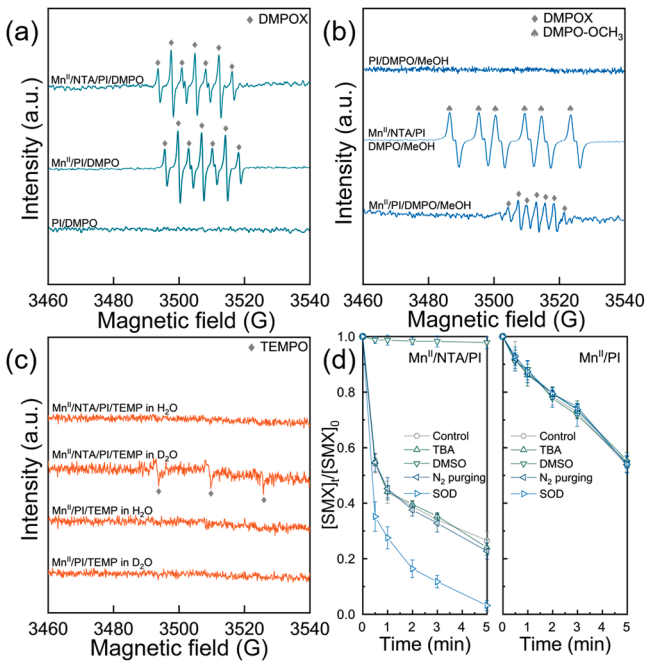

Fig. 4. (a) ESR signal of DMPO products in the Mn^{II}/NTA/PI and Mn^{II}/PI systems. (b) ESR signal of DMPO products in the Mn^{II}/NTA/PI and Mn^{II}/PI systems in methanol. (c) ESR signal for the detection of TEMPO adducts in the Mn^{II}/NTA/PI and Mn^{II}/PI systems in H_2O and D_2O matrix. (d) Degradation of SMX in the Mn^{II}/NTA/PI and Mn^{II}/PI systems in the presence of different scavengers. Conditions: $[SMX]_0 = 20$ μM, $[Mn^{II}]_0 = 20$ μM, $[NTA]_0 = 100$ μM, and $[PI]_0 = 100$ μM; $[TBA]_0 = 20$ mM, $[DMSO]_0 = 2$ mM, $[SOD]_0 = 10^4$ U/L, and pH = 5 (5 mM acetate sodium buffer).
Caption: Due to the ultrafast removal of SMX in the Mn^{II}/NTA/PI system under the experimental conditions presented in Fig. 1. To distinguish the influence of different scavengers, we adjusted the initial concentration of SMX, Mn^{II}, and NTA in these experiments (d).

attributed to the high reactive affinity between high-valent metal-oxo species and sulfoxide substance, so the Mn^{V}-oxo species was rapidly quenched by DMSO. Additionally, nitrogen purging treatment presented a negligible effect on SMX degradation, indicating that the generation of Mn^{V}-oxo species did not require the participation of oxygen. Furthermore, the superoxide dismutase (SOD) for scavenging $^{\bullet}O_2^-$ promoted SMX degradation. We speculated that superoxide exhibited reductive ability which might quench the Mn^{V}-oxo species. Based on the above results of ROS identification, we proposed two possible pathways of PI transformation according to several previous studies [2,58-60]: (i) Mn^{II}-NTA complex was oxidized to Mn^{III}-NTA complex by PI (Eq. 1), and the generated $^{\bullet}IO_3$ could transform to IO_3^- and IO_4^- through spontaneous disproportionation (Eqs. 2 and 3); (ii) $^{\bullet}IO_3$ could react with IO_4^- to generate $^{\bullet}IO_4$ (Eq. d), and $^{\bullet}IO_4$ can be converted to singlet oxygen through self-reaction (Eq. 5).

$$IO_4^- + Mn^{II}\text{-NTA} + 2\,H^+ \uparrow \rightarrow {}^{\bullet}IO_3 + Mn^{III}\text{-NTA} + H_2O \quad (1)$$

$$2\,{}^{\bullet}IO_3 \leftrightarrow I_2O_6 \quad (2)$$

$$I_2O_6 + H_2O \rightarrow IO_3^- + IO_4^- + 2\,H^+ \quad (3)$$

$${}^{\bullet}IO_3 + IO_4^- \rightarrow {}^{\bullet}IO_4 + IO_3^- \quad (4)$$

$$2\,{}^{\bullet}IO_4 \rightarrow 2IO_3^- + {}^1O_2 \quad (5)$$

3.5. Reactive oxidant generated in the Mn^{II}/PI system

3.5.1. Exclusion of the widely proposed transient species

In the absence of NTA, we observed that the Mn^{II}/PI system could also degrade some EOCs without the contribution of Mn^{V}-oxo species, such as SMX, PN, *p*-CP, and BPA (Fig. 1). We deduced that the ROS generation in the Mn^{II}/PI could originate from Mn^{II} ions, PI or their interactions. The potentially generated free radicals were trapped and detected, and the results are shown in Fig. 4a. The obtained ESR signal belonged to DMPOX but not radical-adducts [61-63]. Besides, similar heptad peaks were also presented in the sample taken from the methanol matrix, which could exclude the generation of superoxide radicals (Fig. 4b). In addition, no signal of TEMPO was observed when using TEMP to capture singlet oxygen no matter in D_2O or H_2O solution (Fig. 4c). Moreover, the results of quenching experiments also confirmed the insignificant contribution of the commonly proposed ROS which could be derived from PI or iodate radical (Fig. 4d).

Based on the above results, we speculated that the reactive oxidant generated in Mn^{II}/PI system was more likely to be RMnS derived from Mn^{II} ions. Critical involvement of Mn^{III} species in manganese-based AOPs system has been widely demonstrated due to its redox activity [13,17,64,8]. Theoretically, free aqueous Mn^{III} is unstable and tends to rapid disproportionation to yield the stable Mn^{IV} and Mn^{II} [16,65]. Nevertheless, on account of the complexing ability of iodate and PI [22, 23], it is not rigorous to arbitrarily deny the contribution of Mn^{III} species in the Mn^{II}/PI system. Thus, we obtained the UV–vis spectra of the Mn^{II}/PI process, and we also attempted to acquire complexed Mn^{III} by proportionally mixing Mn^{VII} and Mn^{II} in iodate (IO_3^-) solution for UV–vis spectra analysis (Fig. 5a). However, no characteristic absorption peak in the range of 250 − 300 nm was found in the spectra of the above two samples, indicating that Mn^{III} might not be produced or considering that neither PI nor IO_3^- could coordinate with Mn^{III} species to form stabilized Mn^{III}-ligand complex. Except for Mn^{III} species, the potentially generated manganese species (i.e., Mn^{IV}, Mn^{VI}, and Mn^{VII}) in the Mn^{II}/PI system also exhibit oxidation ability against various organic pollutants, which could be remaining candidates for RMnS that might account for the EOCs oxidation.

3.5.2. Generation and involvement of the nascent colloidal Mn^{IV}

Comparing the UV–vis spectra of Mn^{II}/PI, Mn^{IV}, Mn^{VI}, and Mn^{VII} (Fig. 5**b**), we confirmed that the oxidation products of Mn^{II} ions in the Mn^{II}/PI system were supposed to be the colloidal MnO_2 (i.e., Mn^{IV}). Besides, the colour of Mn^{VI} and Mn^{VII} solution was green and purple, respectively, which was different from the Mn^{II}/PI binary solution (Fig. S5). Besides, we monitored the absorbance of the mixture of Mn^{II} and PI solution at 345 nm within the initial 3 min, and the results prove the generation of colloidal MnO_2 in the Mn^{II}/PI system (Fig. S6). Mainly, MnO_2 (Mn^{IV}) could act as an activator to enhance the oxidation performance of some oxidants, such as permanganate and PMS [8,66]. Thus, we deduced that a similar catalytic oxidation process might also occur in the Mn^{II}/PI system. To verify the above hypothesis, we systematically investigate the degradation kinetics of EOCs in the Mn^{II}/PI system. Interestingly, we observed a self-accelerating trend during the degradation of selected EOCs during the initial stage of the reaction. The plots of $-\ln([EOCs]_t/[EOCs]_0)$ versus reaction time presented a nonlinear pattern, and the tangent slope increased with reaction time

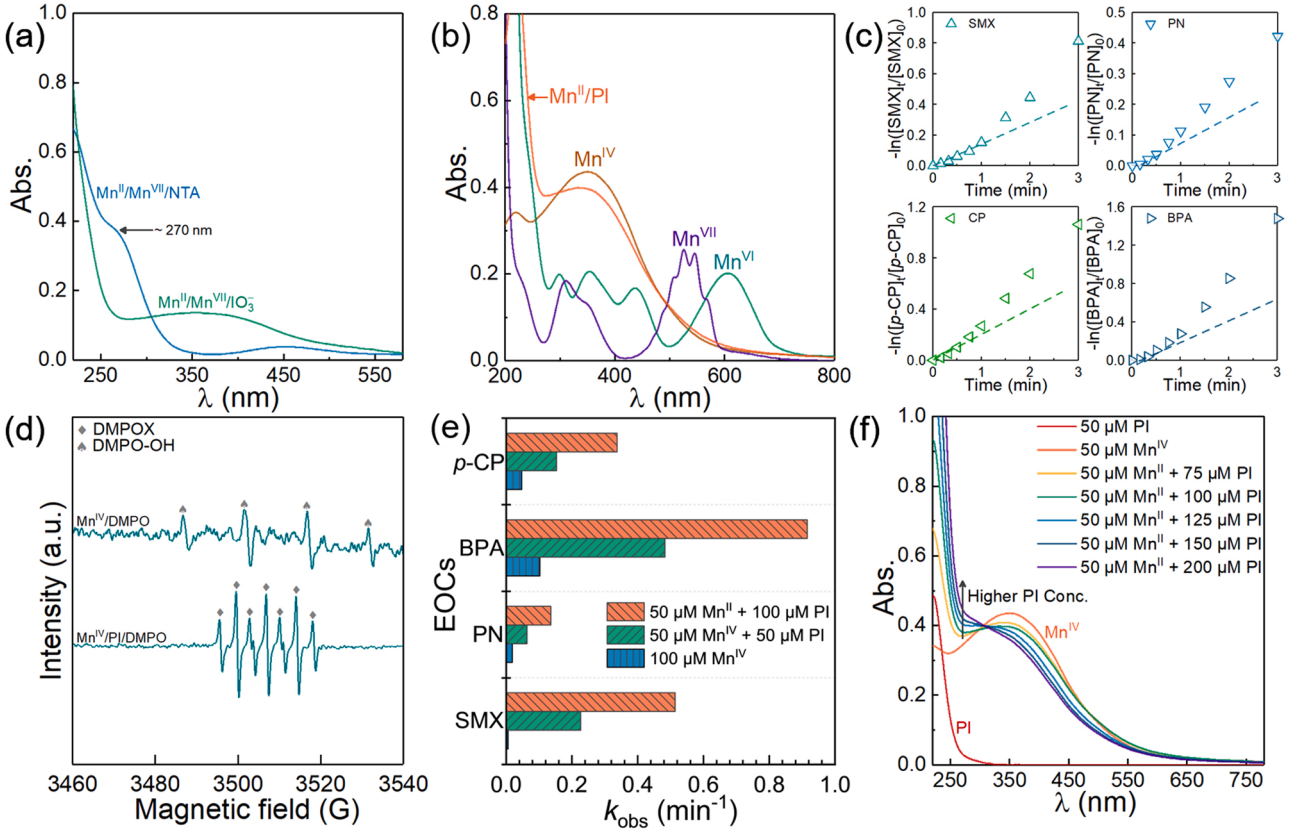

Fig. 5. (a) UV–vis spectra of the mixture of Mn^{II} and Mn^{VII} in NTA solution or iodate (IO_3^-) solution. Conditions: $[Mn^{II}]_0 = 40$ μM, $[Mn^{VII}]_0 = 10$ μM, $[NTA]_0 = [IO_3^-]_0 = 250$ μM. (b) UV–vis spectra of 50 μM Mn^{IV}, 150 μM Mn^{VI}, 100 μM Mn^{VII}, and the mixture of Mn^{II}/PI ($[Mn^{II}]_0 = 50$ μM, $[PI]_0 = 100$ μM). (c) Reaction kinetics of Mn^{II}/PI system with four selected EOCs in the initial 3 min. Conditions: $[EOCs]_0 = 10$ μM, $[Mn^{II}]_0 = 50$ μM, and $[PI]_0 = 100$ μM. pH = 5 (5 mM acetate sodium buffer). (d) ESR signals of DMPO adducts in MnO_2 colloid (Mn^{IV}) and the Mn^{IV}/PI system, respectively. Conditions: $[Mn^{IV}]_0 = 0.2$ mM, $[PI]_0 = 0.4$ mM, and 10 μL DMPO was added into 5 mL sample. (e) Degradation rate constants (k_{obs}) of the selected EOCs in different oxidation systems. Condition: $[EOCs]_0 = 10$ μM, pH 5 (5 mM acetate sodium buffer). (f) UV–vis spectra of the serial Mn^{II}/PI mixture with different PI concentration.

(Fig. 5**c**). This self-accelerating phenomenon was consistent with the generation of Mn^{IV} during the reaction of Mn^{II} ions and PI within the initial 2 min (Figs. S5-S6), which could be attributed to the in-situ formed colloidal MnO_2 (Mn^{IV}) participating in PI activation, thus promoting the degradation of EOCs. Comparatively, in the presence of NTA, Mn^{II} complex was inclined to transform to Mn^{III} complex rather than colloidal MnO_2 (Fig. S7).

However, the role of Mn^{IV} during EOCs oxidation was still unclear. According to the previous studies [8,10], we deduced that Mn^{IV} might act as a catalyst or co-oxidant during PI activation to enhance the removal of selected EOCs. To distinguish the above two possible mechanisms, we attempted to use DMPO as a chemical probe to investigate the oxidation features of Mn^{IV} and the Mn^{IV}/PI system, based on the fact that different DMPO products could present diverse ESR signals. Thus, we analyzed the ESR signals of the DMPO products oxidized by Mn^{IV} and the Mn^{IV}/PI system. As shown in Fig. 5**d**, the characteristic peaks of the DMPO-OH adduct (1:2:2:1) were observed when DMPO was oxidized by colloidal MnO_2 (Mn^{IV}). In view of the inconsiderable existence of $^{\bullet}OH$ in the colloidal MnO_2, we speculated that the formation of DMPO-OH adduct was mediated by Mn^{IV}. Similar to the case of Mn^{VII} and Fe^{IV} [41], the formation of the DMPO-OH adduct could be explained by the Forrester-Hepburn mechanism [67,68], in which DMPO was converted into DMPO-OH^- by the nucleophilic addition of water and subsequently transformed to DMPO-OH adduct under the catalysis of transition metals. However, the signal of DMPOX was detected in the sample of DMPO/Mn^{IV}/PI, which could be ascribed to the direct oxidation of DMPO by strong oxidative intermediates, similar to the DMPO/Mn^{II}/PI system (Fig. 4a).

Moreover, we comparatively employed the Mn^{II}/PI and Mn^{IV}/PI systems to oxidize SMX, PN, *p*-CP, and BPA, and the apparent rate constants (k_{obs}) are presented in Fig. 5e. As shown in Fig. S8, the degradation efficiencies of the selected EOCs in the Mn^{IV}/PI system were faster than that in the Mn^{II}/PI system during the initial reaction, which was probably due to the oxidation process in the Mn^{II}/PI system was triggered by the delayed generation of Mn^{IV}. However, the Mn^{II}/PI system exhibited higher degradation efficiencies of EOCs in the latter reaction, suggesting that the nascent Mn^{IV} for activating PI presented a better performance than the prepared Mn^{IV}. Furthermore, the oxidation performance of the Mn^{II}/PI system was significantly more potent than colloidal MnO_2 alone (Fig. S8), indicating that the RMnS generated in the Mn^{II}/PI was more powerful than Mn^{IV} (colloidal MnO_2).

3.5.3. Identification of the persistent RMnS

These results collectively indicated that some novel reactive oxidant was generated in the Mn^{IV}/PI process mainly because of the role of Mn^{IV} as a catalyst, which was proved by the different oxidation products of the chemical probe (i.e., DMPO). In order to confirm the involvement of Mn^{IV}, UV–vis absorption spectra at 200–800 nm of the serial Mn^{II}/PI binary systems were monitored. As shown in Fig. S9a, the UV–vis spectra of PI and Mn^{IV} colloid presented the maximum absorption peaks near ~221 nm and ~348 nm, respectively. The deconvolution results of the serial UV–vis spectra of Mn^{II}/PI system are shown in Fig. S9b. Notably, with the higher dosages of PI, the absorbance peak of Mn^{IV} presented a blue-shift from ~335 nm to ~276 nm, which provided evidence for the complexation between Mn^{IV} and PI. Besides, with the lower concentration of PI, the absorbance peak of PI also presented a blue-shift from ~220 nm to ~209 nm. It is not difficult to understand that the higher dosage of PI resulted in the higher PI residue; however, total content of the nascent Mn^{IV} was fixed (~50 μM), so the blue-shift caused by the interference of Mn^{IV} became weaker. Therefore, we speculated that the dominant RMnS potentially generated from the Mn^{II}/PI system might be the Mn^{IV}-PI* complex. Based on the above results, we proposed a possible oxidation mechanism in the Mn^{II}/PI system: Mn^{II} ions were firstly oxidized to colloidal MnO_2 by PI, and the nascent colloidal MnO_2 could in turn activate PI to form Mn^{IV}-PI* complex for the degradation of EOCs from water. The above-proposed pathways of PI activation mediated by Mn^{II} ions and complexed Mn^{II} (NTA as an appropriate ligand) are presented in Scheme 1**a**, and the proposed chemical structures of Mn^{II}-NTA complex, Mn^{III}-NTA complex, Mn^{V}-oxo species, and Mn^{IV}-PI* intermediates were presented in Scheme 1b.

3.6. Influencing factors and the potentially generated iodine products

Fig. S10 comparatively presents the degradation of SMX in the Mn^{II}/PI and Mn^{II}/NTA/PI systems under different pH conditions. With the increasing pH from 3.0 to 8.5, the degradation efficiency of SMX in the Mn^{II}/PI system firstly increased and then decreased. We deduced that pH influences the oxidation process through the combined effects on the stability and oxidation ability of the Mn^{IV}-PI* complex. Theoretically, oxidant behaves with more vital oxidation ability under acid conditions; however, a higher concentration of H^+ will also weaken the stability of the complex via the acidic effect. Therefore, the Mn^{II}/PI system exhibited satisfactory performance near-neutral pH (pH 5.9 and 7.2 in our experiments). With regards to the Mn^{II}/NTA/PI system, the activating ability of the Mn^{II} complex attenuated with the increasing pH, which could be attributed to the oxidation ability of Mn^{V}-oxo species being more powerful under acidic conditions. Not coincidentally, similar phenomena were also observed during the EOCs degradation dominated by other high-valent metal-oxo species (e.g., Fe^{IV}, Co^{IV} and Cr^{V}) [31,39,44]. Furthermore, sulfoxide transformation experiments were carried out to examine whether the reactive oxidant was pH-dependent. As shown in Fig. 6a, the yield of $PMSO_2$ substantially increased from ~88 % to ~96 %, with solution pH increasing from 3.0 to 5.8, and then decreased to ~84 % with the solution pH further increasing to 8.5. Though some other ROS was potentially generated under acidic or weak-alkaline conditions, the Mn^{V}-oxo species was still the dominant oxidant within pH range from 3.0 to 8.5. Moreover, we monitored the pH variation during PI activation via hydrated and complexed Mn^{II} without buffer, as shown in Fig. S11. pH of the Mn^{II}/NTA/PI system was relatively stable, while the pH of the Mn^{II}/PI system decreased from ~5.0 to ~4.2 within the initial 2 min, which could be attributed to the hydrolysis of the nascent colloidal Mn^{IV}.

Additionally, Cl^- and NO_3^- presented negligible effects on the degradation of SMX (Fig. S12), indicating that the Mn^{V}-oxo species was resistant to the interferences of these anions. Moreover, dissolved organic matter (humic acid (HA) as a model compound here) slightly influenced SMX degradation. We speculated that the influence of HA mainly consisted of the following two aspects [1,10]: (i) reductive groups on HA molecule could compete with reactive species and result in the inhibition; (ii) some oxygen-containing groups on HA molecule could complex with Mn which might stabilize the generated RMnS to enhance their oxidation ability.

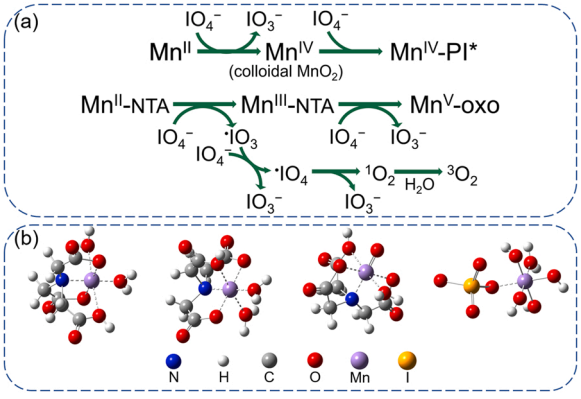

Scheme 1. (a) Proposed pathways for PI activation mediated by Mn^{II} ions and Mn^{II}-NTA complex. (b) Proposed chemical structures of Mn^{II}-NTA complex, Mn^{III}-NTA complex, Mn^{V}-oxo species, and Mn^{IV}-PI* complex (from left to right).

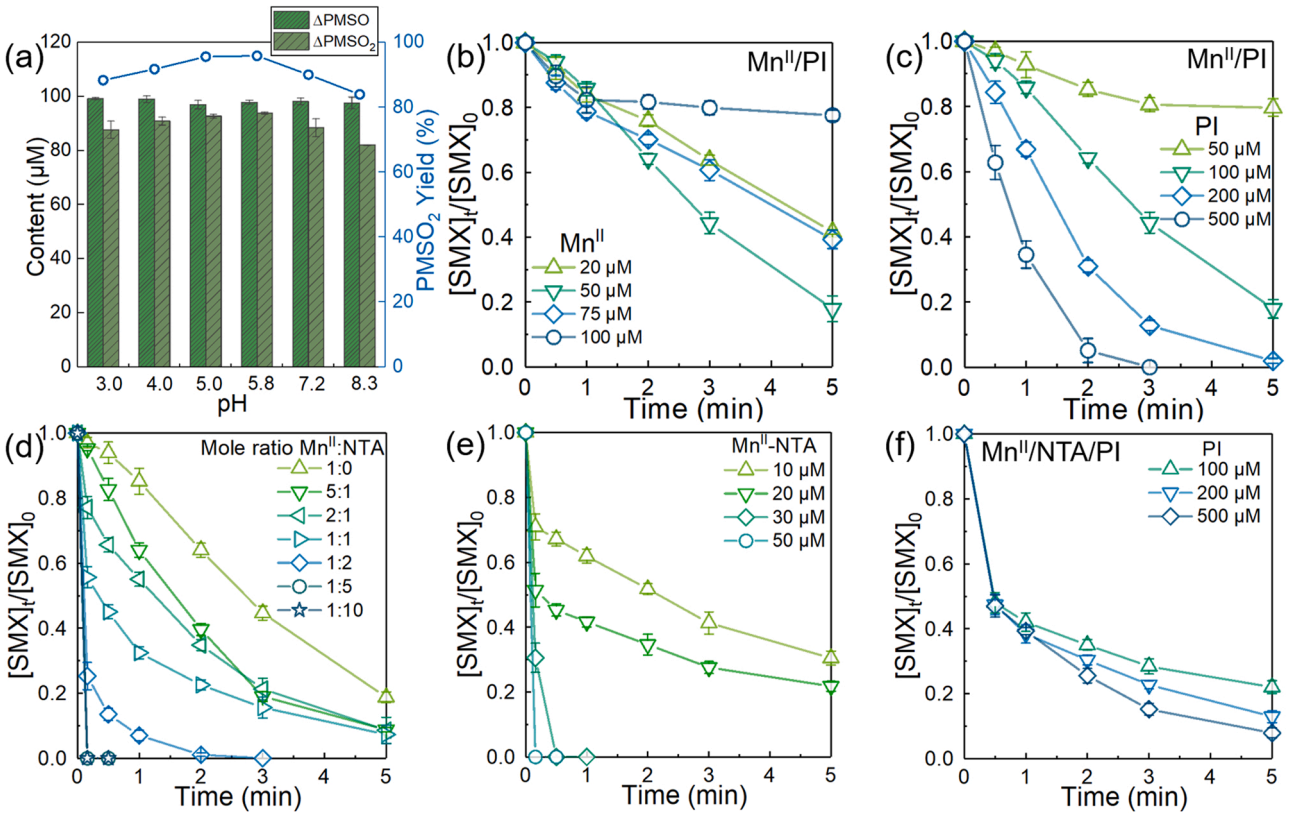

Fig. 6. (a) Effects of pH on PMSO consumption and $PMSO_2$ generation in the Mn^{II}/NTA/PI system. Conditions: $[PMSO]_0 = 100$ μM, $[Mn^{II}]_0 = 50$ μM, $[NTA]_0 = 250$ μM, $[PI]_0 = 200$ μM, and Time = 3 min. There was no buffer in the reaction solution with pH 3.0. The reaction solution with pH 4.0, 5.0, and 5.8 contained 5 mM of acetate sodium buffer. The reaction solution with pH 7.2 and 8.3 contained 5 mM of borate sodium buffer. (b and c) Effect of reagent concentration on the degradation of SMX in the Mn^{II}/PI system. Conditions: (b) $[SMX]_0 = 10$ μM and $[PI]_0 = 100$ μM. (c) $[SMX]_0 = 10$ μM and $[Mn^{II}]_0 = 50$ μM. All experiments were carried out under pH 5 (5 mM acetate sodium buffer). (d, e and f) Effect of reagent concentration on the degradation of SMX in the Mn^{II}/NTA/PI system. Conditions: (d) $[SMX]_0 = 10$ μM, $[PI]_0 = 100$ μM, and a fixed concentration of $[Mn^{II}]_0 = 50$ μM. (e) $[SMX]_0 = 10$ μM, $[PI]_0 = 100$ μM, and a fixed mole ratio of $[Mn^{II}]_0$:$[NTA]_0$ at 1:5. (f) $[SMX]_0 = 20$ μM, $[Mn^{II}]_0 = 20$ μM, and $[NTA]_0 = 100$ μM. All experiments were carried out under pH 5 (5 mM acetate sodium buffer).

Furthermore, we investigated the influence of reagent dosage on SMX degradation in both oxidation systems (Fig. 6b-f). In the Mn^{II}/PI system, the degradation efficiency of SMX increased as the Mn^{II} concentration increased from 20 to 50 μM, while the enhancement was weakened as the Mn^{II} concentration further increased to 100 μM (Fig. 6b). This might be due to the consumption of PI caused by Mn^{II}. Mn^{II} ions were first oxidized to Mn^{IV}, and then Mn^{IV} participated in PI activation, which contributed to the degradation of SMX. Excessive Mn^{II} could competitively consume PI and result in the decrease of Mn^{IV}-PI* generation as the reactive oxidant. Besides, removal of SMX was significantly accelerated with the PI dosage ranging from 50 to 500 μM (Fig. 6c), which could be attributed to the fact that the increase of PI concentration was conducive to the formation of Mn^{IV}-PI* complex. Moreover, the degradation efficiency of SMX in the Mn^{II}/NTA/PI system monotonously increased with the increasing NTA dosage (Fig. 6d), which could be attributed to the stability of RMnS being affected by the mole ratio of $[Mn^{II}]$:[NTA]. In addition, Fig. 6e presents the degradation of SMX in the presence of different Mn^{II} concentrations at a fixed mole ratio of $[Mn^{II}]$:[NTA], suggesting that the oxidation of SMX was significantly enhanced with increasing Mn^{II}-NTA concentration. Briefly, as the Mn^{II}-NTA dosages increased from 10 to 50 μM, the percentage of SMX degradation increased from ~30 % to ~100 % within the first 10 s. It was not difficult to understand that the increasing RMnS generation could accelerate the oxidation of SMX. However, the oxidation of SMX in the first 10 s was barely affected by increasing PI dosages (Fig. 6**f**), which was different from the Mn^{II}/PI system. Combined with the identification of Mn^{V}-oxo species as the dominant RMnS in the previous discussion, this negligible effect of PI concentration indicated that the generation of Mn^{V} intermediates originating from the Mn^{III} complex might be the rate-limiting step of the EOCs degradation in the Mn^{II}/NTA/PI system [32].

The possibly generated by-products during PI activation were determined in the Mn^{II}/PI and Mn^{II}/NTA/PI systems, such as I_2, I_3^-, and HOI, which possess potential environmental risks in forming highly toxic iodinated by-products in water treatment processes. Excessive phenol was introduced as the probe compound to capture the potentially generated HOI because HOI could readily react with phenol to generate iodinated phenols, including 2-iodophenol (2-IP) and 4-iodophenol (4-IP) [26,31]. As shown in Fig. S13, the generation of HOI in both oxidation systems could be excluded due to the undetected 2-IP and 4-IP. Besides, I_2/I_3^- were determined by a starch colorimetric method, and neither I_2 nor I_3^- was detected in both oxidation systems (Fig. S14).

3.7. Degradation pathways of SMX in the different oxidation processes

The intermediates produced from SMX degradation in the Mn^{II}/PI and Mn^{II}/NTA/PI systems were identified to further investigate the interaction between SMX and Mn^{IV}-PI* complex or Mn^{V}-oxo species. To sum up, eleven degradation products of SMX (including SMX) were detected, of which eight were further identified by MS/MS [2] analysis (Figs. S15-S22), and the chemical structures of the eleven degradation intermediates are listed in Table S2. Generally, SMX degradation in both oxidation systems mainly followed four patterns: amino oxidation, N-centred radical coupling, N–S bond cleavage, and hydroxylation, which were similar to the degradation pathways of SMX mediated by Fe^{IV}-oxo and Co^{IV}-oxo species [31,40]. The amino group (–NH_2, TP 253)

could be oxidized to nitro-products (–NO_2, TP 283) through the O-addition pathway, corresponding to the generation of hydroxyamino-products (–NHOH, TP 269) and nitroso-products (–NO, TP 267) as intermediates. Besides, the dimeric products (i.e., TP 502, TP 347, and TP 192) could be produced by the coupling of N-centred radicals originating from the H abstraction reaction on the amino groups, and TP 518 was the hydroxylated product subsequently generated from TP 502. Additionally, TP 98 could be generated from SMX via the N–S bond cleavage. Gaussian 16 W software was used to optimize the structure and calculate the wave function of SMX at the B3LYP/6–31 G (d, p) level. The IEFPCM was used in the calculation process, and water was chosen as the solvent. The optimized structures and orbitals/isosurfaces of SMX molecule were shown in Fig. 7a-h, and the detailed discussion was presented in **Text S6** and Table S3. In general, the results of theoretical calculation indicated that the N25 belonging to –NH_2 was more easily attacked by electrophilic species. Thus, the amino group on SMX molecule preferred to reacted with RMnS to undergo oxidation process, such as radical-coupling, hydroxyl substitution, and O-addition pathways, which were consistent with the results of UPLC-MS/MS^2 analysis. To assess potential risks of the degradation products, QSAR analysis was performed using the ECOSAR program and T.E.S.T. software to evaluate the toxicity of SMX and its degradation products. As shown in Fig. S23, the identified degradation products possessed toxicities similar to that of SMX. Nevertheless, the active sites of SMX (aniline groups) have been destructed, so the degradation products might not exhibit antibacterial activity.

We monitored the product evolution during SMX degradation by collecting samples from the Mn^{II}/NTA/PI system at time intervals of 10 s, 30 s, and 60 s; and the Mn^{II}/PI system at 5 min, 10 min, and 20 min, respectively. Notably, comparing the detection results of all the samples taken among both oxidation processes (Fig. 7i), we found some subtle differences between the degradation pathways of SMX mediated by Mn^{V}-oxo species and Mn^{IV}-PI* complex. The hydroxyamino-products (–NHOH, TP 269) and the nitroso-products (–NO, TP 267) were all detected in both systems; however, the nitro-products (–NO_2, TP 283) were only detected in the Mn^{II}/NTA/PI system, indicating that the nitroso group could be further oxidized to nitro group by the highly reactive Mn^{V}-oxo species. The transformation from TP 267 to TP 283 was considered to be the oxidation of the nitroso group to the nitro group via an oxygen-atom transfer step mediated by high-valent metal-oxo species, which supported the critical contribution of Mn^{V}-oxo species in the Mn^{II}/NTA/PI system. Moreover, the nitroso group could be generated from the amino group via hydroxy-substitute and dehydration pathways [69,70], which were capable of induced by the Mn^{IV}-PI* complex produced by the Mn^{II}/PI process. In addition, we found that the Mn^{V}-oxo species could mediate the substitution of the amino group by the hydroxy group, resulting in the formation of TP 254, which was impracticable in the Mn^{II}/PI system. The proposed degradation pathways of SMX in both oxidation systems are presented in Fig. 7j.

3.8. Applications for water treatment

Compared with the radical-based AOPs, Mn^{V}-oxo species presented good resistance against complex water matrices, such as halogen ions, oxyanions, and dissolved organic matter (DOM). We applied the Mn^{II}/NTA/PI oxidation system to the actual water (i.e., reservoir water and domestic sewage), and the main matrix characteristics were listed in Text S7. As shown in Fig. S24, the proposed oxidation technology could efficiently degrade SMX under the disturbance of complex water matrices due to the selective oxidation feature of RMnS. Considering the biodegradability of NTA and the non-toxic iodate (IO_3^-) products generated from PI, AOPs based on the Mn^{II}/NTA/PI system could be applicable for the pre-oxidation of industrial effluents and/or pharmaceutical wastewater containing refractory organic contaminants (e.g., halophenols and antibiotics) to improve their biodegradability, or for advanced sewage treatment to selectively degrade EOCs under DOM background.

Besides, we monitored the consumption of PI and NTA during SMX degradation in the Mn^{II}/NTA/PI system (Fig. S25). NTA was relatively stable during SMX degradation, which indicated that the Mn^{II}/NTA/PI system should be catalytic. We chose PMSO as the target compound to examine the turnover frequency of the Mn^{V}-oxo species because the consumption of PMSO and PI strictly followed a stoichiometric relationship, which is capable of undertaking mass balance during cycle oxidation processes. The results suggested that the stabilized Mn^{III}-NTA complex could act as a catalyst during the continuous generation of

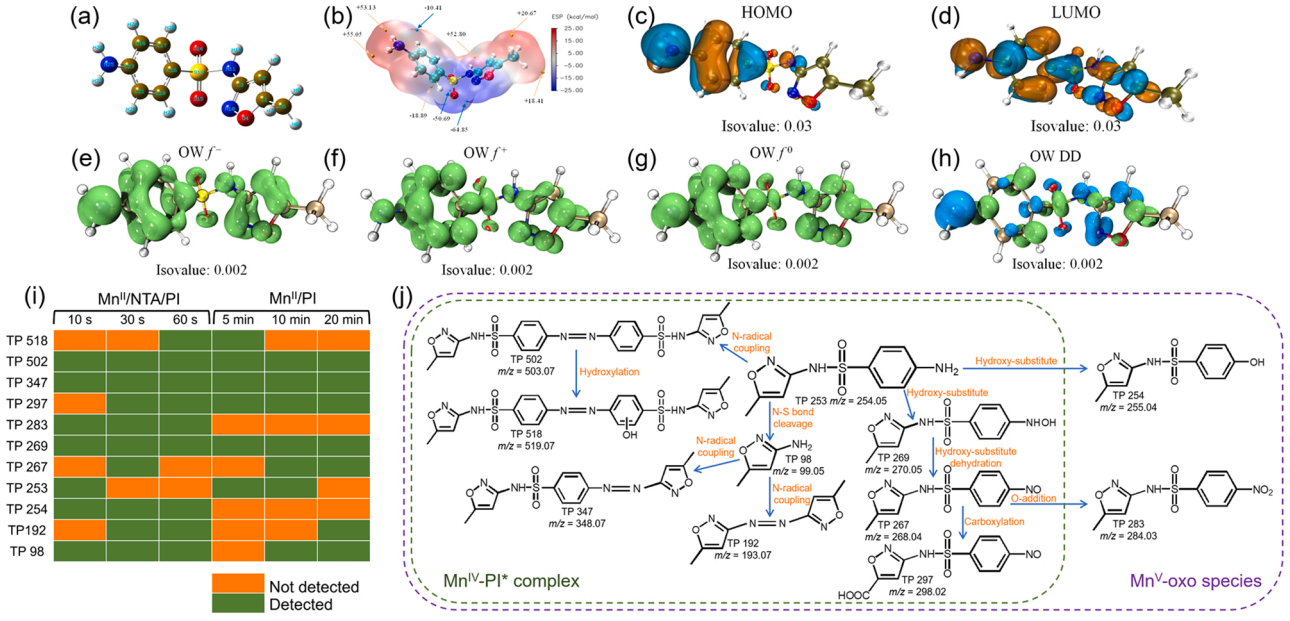

Fig. 7. Optimized structure at B3LYP/6–31 G(d, p) level using IEFPCM (a), ESP (b), HOMO (c), LUMO (d), the isosurface of orbital weighted Fukui functions (e)-(g) and orbital weighted dual descriptors (h) of SMX. (i) Detection of the degradation products during SMX degradation in the Mn^{II}/PI and Mn^{II}/NTA/PI systems. Conditions: $[SMX]_0$ = 20 μM, $[Mn^{II}]_0$ = 50 μM, $[NTA]_0$ = 250 μM, $[PI]_0$ = 200 μM, and pH = 5 (5 mM acetate sodium buffer). (j) Schematic illustration of the proposed pathways for SMX degradation dominated by Mn^{IV}-PI* complex and high-valent Mn^{V}-oxo species.

Mn^{V}-oxo species (Fig. S26). During the sixth oxidation test, ~70% of PMSO was oxidized to $PMSO_2$ within 30 s. Thus, the stability of NTA during the generation of RMnS might inspire the designing of catalyst modification, changing the oxidation process from the liquid phase to the interface, which is conducive to the separation of metal ions and ligands from the water after the reaction.

4. Conclusions and Outlook

This work introduced nitrogenous carboxylic acid (i.e., nitrilotriacetic acid, NTA) as functional ligands of soluble Mn^{II} for periodate (IO_4^-, PI) activation, constituting a novel catalytic oxidation technology that could oxidize multiple organic contaminants and achieve a removal efficiency of ~99% within seconds. The proposed non-radical catalytic oxidation system exhibited satisfactory resistance against complex water matrices, such as chloride, bicarbonate, natural organic matter (NOM), and effluent organic matter (EfOM). Moreover, unwanted iodine products (e.g., HOI, I_2, and I_3^-) potentially generated from IO_4^- were not detected in both Mn^{II}/PI system and Mn^{II}/NTA/PI system.

There are still some limitations and challenges that warrant further study. First, we found that different ligands exhibited disparate effects on the oxidation performance of PI activated by the complexed Mn^{II}, so clarifying the influence of different ligands on the generation and oxidation ability of RMnS requires more deliberation, such as the configuration of metal-ligands complex or the degradation of reductive ligands. Besides, the origin of the selective oxidation for EOCs elimination by RMnS remains unclear, which probably correlated to the generation of unstable complexed intermediates for the interspecies target electron transfer. Therefore, more efforts are needed to deepen the understanding of the Mn valence shift triggered by the combination of ligands and oxidants to achieve sustained and complete contaminant oxidation during water treatment.

CRediT authorship contribution statement

Yingxu Gong: Conceptualization, Investigation, Data curation, Writing – original draft. **Jimin Shen:** Methodology, Validation. **Yining Wu:** Supervision, Validation. **Linlu Shen:** Software, Methodology. **Shengxin Zhao:** Supervision, Software, Writing – review & editing, Methodology. **Yanchi Zhou, Yabin Li, Lei Cui:** Data curation, Methodology. **Jing Kang:** Supervision. **Zhonglin Chen:** Conceptualization, Supervision, Funding acquisition, Writing – review & editing, Validation.

Declaration of Competing Interest

The authors declare that they have no known competing financial interests or personal relationships that could have appeared to influence the work reported in this paper.

Data Availability

The data that support this study are available from the corresponding author upon reasonable request.

Acknowledgments

This work was supported by the National Key Research and Development Program of China (2019YFD1100104); Heilongjiang Touyan Innovation Team Program (HIT-SE-01); the National Natural Science Foundation of China (52000047; 51608148); the Open Project of State Key Laboratory of Urban Water Resource and Environment, Harbin Institute of Technology (QA201817); and Postdoctoral Scientific Research Developmental Fund of Heilongjiang Province (LBH-Q18061). We acknowledge all the members of Zhonglin Research Group for valuable discussions, especially Qianqian Jin, Xiaoxiao Zhang, Lanbo Bi, Xiaotong Xu, Chao Chen, and Yanbin Tong.

Appendix A. Supporting information

Supplementary data associated with this article can be found in the online version at doi:10.1016/j.apcatb.2022.122093.

References

[1] J. Li, S. Pang, Z. Wang, Q. Guo, J. Duan, S. Sun, L. Wang, Y. Cao, J. Jiang, Oxidative transformation of emerging organic contaminants by aqueous permanganate: kinetics, products, toxicity changes, and effects of manganese products, Water Res. 203 (2021), 117513.
[2] J. Lee, U. von Gunten, J. Kim, Persulfate-based advanced oxidation: critical assessment of opportunities and roadblocks, Environ. Sci. Technol. 54 (6) (2020) 3064–3081.
[3] W. Ren, C. Cheng, P. Shao, X. Luo, H. Zhang, S. Wang, X. Duan, Origins of electron-transfer regime in persulfate-based nonradical oxidation processes, Environ. Sci. Technol. 56 (1) (2022) 78–97.
[4] E.L. Trainer, M. Ginder-Vogel, C.K. Remucal, Selective reactivity and oxidation of dissolved organic matter by manganese oxides, Environ. Sci. Technol. 55 (17) (2021) 12084–12094.
[5] S. Zhang, T. Hedtke, L. Wang, X. Wang, T. Cao, M. Elimelech, J. Kim, Engineered nanoconfinement accelerating spontaneous manganese-catalyzed degradation of organic contaminants, Environ. Sci. Technol. 55 (24) (2021) 16708–16715.
[6] S. Laha, R.G. Luthy, Oxidation of aniline and other primary aromatic amines by manganese dioxide, Environ. Sci. Technol. 24 (3) (1990) 363–373.
[7] A.T. Stone, Reductive dissolution of manganese(III/IV) oxides by substituted phenols, Environ. Sci. Technol. 21 (10) (1987) 979–988.
[8] Y. Gao, J. Jiang, Y. Zhou, S. Pang, C. Jiang, Q. Guo, J. Duan, Does soluble Mn(III) oxidant formed in situ account for enhanced transformation of triclosan by Mn(VII) in the presence of ligands? Environ. Sci. Technol. 52 (8) (2018) 4785–4793.
[9] J. Jiang, S. Pang, J. Ma, Role of ligands in permanganate oxidation of organics, Environ. Sci. Technol. 44 (11) (2010) 4270–4275.
[10] B. Sun, J. Zhang, J. Du, J. Qiao, X. Guan, Reinvestigation of the role of humic acid in the oxidation of phenols by permanganate, Environ. Sci. Technol. 47 (24) (2013) 14332–14340.
[11] D. He, X. Guan, J. Ma, M. Yu, Influence of different nominal molecular weight fractions of humic acids on phenol oxidation by permanganate, Environ. Sci. Technol. 43 (21) (2009) 8332–8337.
[12] X. Wang, S. Wang, R. Qu, J. Ge, Z. Wang, C. Gu, Enhanced removal of chlorophene and 17β-estradiol by Mn(III) in a mixture solution with humic acid: investigation of reaction kinetics and formation of co-oligomerization products, Environ. Sci. Technol. 52 (22) (2018) 13222–13230.
[13] S. Zhong, H. Zhang, Mn(III)-ligand complexes as a catalyst in ligand-assisted oxidation of substituted phenols by permanganate in aqueous solution, J. Hazard. Mater. 384 (2020), 121401.
[14] M.R. Jones, G.W. Luther, A. Mucci, B.M. Tebo, Concentrations of reactive Mn(III)-L and MnO_2 in estuarine and marine waters determined using spectrophotometry and the leuco base, leucoberbelin blue, *Talanta* 200 (2019) 91–99.
[15] Y. Sun, J. Im, N. Shobnam, S.K. Fanourakis, L. He, L.M. Anovitz, P.R. Erickson, H. Sun, J. Zhuang, F.E. Löffler, Degradation of adsorbed Bisphenol A by soluble Mn (III), Environ. Sci. Technol. (2021), acs.est.1c03862.
[16] J.K. Klewicki, J.J. Morgan, Kinetic behavior of Mn(III) complexes of pyrophosphate, EDTA, and citrate, Environ. Sci. Technol. 32 (19) (1998) 2916–2922.
[17] J. Jiang, S. Pang, J. Ma, Oxidation of triclosan by permanganate (Mn(VII)): importance of ligands and in situ formed manganese oxides, Environ. Sci. Technol. 43 (21) (2009) 8326–8331.
[18] J. Jiang, Y. Gao, S. Pang, X. Lu, Y. Zhou, J. Ma, Q. Wang, Understanding the role of manganese dioxide in the oxidation of phenolic compounds by aqueous permanganate, Environ. Sci. Technol. 49 (1) (2015) 520–528.
[19] B. Sun, X. Guan, J. Fang, P.G. Tratnyek, Activation of manganese oxidants with bisulfite for enhanced oxidation of organic contaminants: the involvement of Mn (III), Environ. Sci. Technol. 49 (20) (2015) 12414–12421.
[20] Y. Gao, Y. Zhou, S. Pang, J. Jiang, Z. Yang, Y. Shen, Z. Wang, P. Wang, L. Wang, New insights into the combination of permanganate and bisulfite as a novel advanced oxidation process: importance of high-valent manganese-oxo species and sulfate radical, Environ. Sci. Technol. 53 (7) (2019) 3689–3696.
[21] C. Guan, Q. Guo, Z. Wang, X. Wei, B. Han, X. Luo, H. Pan, J. Jiang, Bisulfite activated permanganate for oxidative water decontamination, Water Res. 216 (2022), 118331.
[22] Y. Wang, Y. Wu, Y. Yu, T. Pan, D. Li, D. Lambropoulou, X. Yang, Natural polyphenols enhanced the Cu(II)/peroxymonosulfate (PMS) oxidation: the contribution of Cu(III) and HO•, Water Res. 186 (2020), 116326.
[23] L. Wang, H. Xu, N. Jiang, Z. Wang, J. Jiang, T. Zhang, Trace cupric species triggered decomposition of peroxymonosulfate and degradation of organic pollutants: Cu(III) being the primary and selective intermediate oxidant, Environ. Sci. Technol. 54 (7) (2020) 4686–4694.
[24] Y. Choi, H. Yoon, C. Lee, L.U. Vetráková, D. Heger, K. Kim, J. Kim, Activation of periodate by freezing for the degradation of aqueous organic pollutants, Environ. Sci. Technol. 52 (9) (2018) 5378–5385.

[25] L. Chia, X. Tang, L.K. Weavers, Kinetics and mechanism of photoactivated periodate reaction with 4-chlorophenol in acidic solution, Environ. Sci. Technol. 38 (24) (2004) 6875–6880.

[26] F. Liu, Z. Li, Q. Dong, C. Nie, S. Wang, B. Zhang, P. Han, M. Tong, Catalyst-free periodate activation by solar irradiation for bacterial disinfection: performance and mechanisms, Environ. Sci. Technol. 56 (7) (2022) 4413–4424.

[27] H. Sun, F. He, W. Choi, Production of reactive oxygen species by the reaction of periodate and hydroxylamine for rapid removal of organic pollutants and waterborne bacteria, Environ. Sci. Technol. 54 (10) (2020) 6427–6437.

[28] A.D. Bokare, W. Choi, Singlet-oxygen generation in alkaline periodate solution, Environ. Sci. Technol. 49 (24) (2015) 14392–14400.

[29] Y. Long, J. Dai, S. Zhao, Y. Su, Z. Wang, Z. Zhang, Atomically dispersed cobalt sites on graphene as efficient periodate activators for selective organic pollutant degradation, Environ. Sci. Technol. 55 (8) (2021) 5357–5370.

[30] H. Lee, H. Yoo, J. Choi, I. Nam, S. Lee, S. Lee, J. Kim, C. Lee, J. Lee, Oxidizing capacity of periodate activated with iron-based bimetallic nanoparticles, Environ. Sci. Technol. 48 (14) (2014) 8086–8093.

[31] Y. Zong, Y. Shao, Y. Zeng, B. Shao, L. Xu, Z. Zhao, W. Liu, D. Wu, Enhanced oxidation of organic contaminants by Iron(II)-activated periodate: the significance of high-valent iron–oxo species, Environ. Sci. Technol. 55 (11) (2021) 7634–7642.

[32] Y. Gao, Y. Zhou, S. Pang, J. Jiang, Y. Shen, Y. Song, J. Duan, Q. Guo, Enhanced peroxymonosulfate activation via complexed Mn(II): a novel non-radical oxidation mechanism involving manganese intermediates, Water Res. 193 (2021), 116856.

[33] B.H. Pfeil, G.F. Lee, Biodegradation of nitrilotriacetic acid in aerobic systems, Environ. Sci. Technol. 2 (7) (1968) 543–546.

[34] A. Ndjou'Ou, J. Bou-Nasr, D. Cassidy, Effect of fenton reagent dose on coexisting chemical and microbial oxidation in soil, Environ. Sci. Technol. 40 (8) (2006) 2778–2783.

[35] C.R. Keenan, D.L. Sedlak, Ligand-enhanced reactive oxidant generation by nanoparticulate zero-valent iron and oxygen, Environ. Sci. Technol. 42 (18) (2008) 6936–6941.

[36] Frisch, M.J.; Trucks, G.W.; Schlegel, H.B.; Scuseria, G.E.; Robb, M.A.; Cheeseman, J.R.; Scalmani, G.; Barone, V.; Petersson, G.A.; Nakatsuji, H.; Li, X.; Caricato, M.; Marenich, A.V.; Bloino, J.; Janesko, B.G.; Gomperts, R.; Mennucci, B.; Hratchian, H.P.; Ortiz, J.V.; Izmaylov, A.F.; Sonnenberg, J.L.; Williams; Ding, F.; Lipparini, F.; Egidi, F.; Goings, J.; Peng, B.; Petrone, A.; Henderson, T.; Ranasinghe, D.; Zakrzewski, V.G.; Gao, J.; Rega, N.; Zheng, G.; Liang, W.; Hada, M.; Ehara, M.; Toyota, K.; Fukuda, R.; Hasegawa, J.; Ishida, M.; Nakajima, T.; Honda, Y.; Kitao, O.; Nakai, H.; Vreven, T.; Throssell, K.; Montgomery Jr., J.A.; Peralta, J.E.; Ogliaro, F.; Bearpark, M.J.; Heyd, J.J.; Brothers, E.N.; Kudin, K.N.; Staroverov, V.N.; Keith, T.A.; Kobayashi, R.; Normand, J.; Raghavachari, K.; Rendell, A.P.; Burant, J.C.; Iyengar, S.S.; Tomasi, J.; Cossi, M.; Millam, J.M.; Klene, M.; Adamo, C.; Cammi, R.; Ochterski, J.W.; Martin, R.L.; Morokuma, K.; Farkas, O.; Foresman, J.B.; Fox, D.J., Gaussian 16W, 2016.

[37] J. Zhang, T.L. efficient evaluation of electrostatic potential with computerized optimized code, Phys. Chem. Chem. Phys. 23 (2021) *20323–20328*.

[38] T. Lu, F.C. Multiwfn: a multifunctional wavefunction analyzer, J. Comput. Chem. 22 (2012) *580–592*.

[39] W. Humphrey, A.D. K.S, VMD: visual molecular dynamics, J. Mol. Graph. 14 (1996) *33–38*.

[40] Y. Zong, X. Guan, J. Xu, Y. Feng, Y. Mao, L. Xu, H. Chu, D. Wu, Unraveling the overlooked involvement of high-valent cobalt-oxo species generated from the cobalt(II)-activated peroxymonosulfate process, Environ. Sci. Technol. 54 (24) (2020) 16231–16239.

[41] Z. Wang, J. Jiang, S. Pang, Y. Zhou, C. Guan, Y. Gao, J. Li, Y. Yang, W. Qiu, C. Jiang, Is sulfate radical really generated from peroxydisulfate activated by Iron (II) for environmental decontamination? Environ. Sci. Technol. 52 (19) (2018) 11276–11284.

[42] H.M. Neu, T. Yang, R.A. Baglia, T.H. Yosca, M.T. Green, M.G. Quesne, S.P. de Visser, D.P. Goldberg, Oxygen-atom transfer reactivity of axially ligated Mn(V)–oxo complexes: evidence for enhanced electrophilic and nucleophilic pathways, J. Am. Chem. Soc. 136 (39) (2014) 13845–13852.

[43] N. Jiang, H. Xu, L. Wang, J. Jiang, T. Zhang, Nonradical oxidation of pollutants with single-atom-Fe(III)-activated persulfate: Fe(V) being the possible intermediate oxidant, Environ. Sci. Technol. 54 (21) (2020) 14057–14065.

[44] B. Liu, W. Guo, W. Jia, H. Wang, Q. Si, Q. Zhao, H. Luo, J. Jiang, N. Ren, Novel nonradical oxidation of sulfonamide antibiotics with Co(II)-doped g-C_3N_4 activated peracetic acid: role of high-valent cobalt-oxo species, Environ. Sci. Technol. 55 (18) (2021) 12640–12651.

[45] H. Dong, G. Wei, T. Cao, B. Shao, X. Guan, T.J. Strathmann, Insights into the oxidation of organic cocontaminants during Cr(VI) reduction by sulfite: the overlooked significance of Cr(V), Environ. Sci. Technol. 54 (2) (2020) 1157–1166.

[46] O. Pestovsky, S. Stoian, E.L. Bominaar, X. Shan, E. Münck, L. Que, A. Bakac, Aqueous Fe^{IV}=O: spectroscopic identification and oxo-group exchange, Angew. Chem. Int. Ed. 44 (42) (2005) 6871–6874.

[47] U. Maitra, B.S. Naidu, A. Govindaraj, C.N.R. Rao, Importance of trivalency and the eg1 configuration in the photocatalytic oxidation of water by Mn and Co oxides, Proc. Natl. Acad. Sci. U.S.A. 110 (29) (2013) 11704–11707.

[48] D.M. Robinson, Y.B. Go, M. Mui, G. Gardner, Z. Zhang, D. Mastrogiovanni, E. Garfunkel, J. Li, M. Greenblatt, G.C. Dismukes, Photochemical water oxidation by crystalline polymorphs of manganese oxides: structural requirements for catalysis, J. Am. Chem. Soc. 135 (9) (2013) 3494–3501.

[49] T. Takashima, K. Hashimoto, R. Nakamura, Inhibition of charge disproportionation of MnO_2 electrocatalysts for efficient water oxidation under neutral conditions, J. Am. Chem. Soc. 134 (44) (2012) 18153–18156.

[50] Q. Jin, J. Kang, Q. Chen, J. Shen, F. Guo, Z. Chen, Efficiently enhanced Fenton-like reaction via Fe complex immobilized on silica particles for catalytic hydrogen peroxide degradation of 2,4-dichlorophenol, Appl. Catal. B: Environ. 268 (2020), 118453.

[51] H. Li, C. Shan, B. Pan, Fe(III)-doped g-C_3N_4 mediated peroxymonosulfate activation for selective degradation of phenolic compounds via high-valent iron-oxo species, Environ. Sci. Technol. 52 (4) (2018) 2197–2205.

[52] H. Gao, C. Huang, L. Mao, B. Shao, J. Shao, Z. Yan, M. Tang, B. Zhu, First direct and unequivocal electron spin resonance spin-trapping evidence for pH-dependent production of hydroxyl radicals from sulfate radicals, Environ. Sci. Technol. 54 (21) (2020) 14046–14056.

[53] G.S. Timmins, K.J. Liu, E.J.H. Bechara, Y. Kotake, H.M. Swartz, Trapping of free radicals with direct in vivo EPR detection: a comparison of 5,5-dimethyl-1-pyrroline-N-oxide and 5-diethoxyphosphoryl-5-methyl-1-pyrroline-N-oxide as spin traps for $HO^{\bullet}$ and $SO_4^{\bullet-}$, Free Radic. Biol. Med. 27 (3) (1999) 329–333.

[54] Y. Li, Z. Chen, J. Qi, J. Kang, J. Shen, P. Yan, W. Wang, L. Bi, X. Zhang, X. Zhu, Degradation of bisphenol S by peroxymonosulfate activation through monodispersed $CoFe_2O_4$ nanoparticles anchored on natural palygorskite, Sep. Purif. Technol. 277 (2021), 119492.

[55] S. Wang, Z. Chen, P. Yan, T. She, W. Wang, L. Bi, J. Kang, J. Shen, X. Li, L. Shen, Y. Cheng, Enhanced degradation of iohexol in water by $CuFe_2O_4$ activated peroxymonosulfate: efficiency, mechanism and degradation pathway, Chemosphere 289 (2022), 133198.

[56] S. Zhu, X. Li, J. Kang, X. Duan, S. Wang, Persulfate activation on crystallographic manganese oxides: mechanism of singlet oxygen evolution for nonradical selective degradation of aqueous contaminants, Environ. Sci. Technol. 53 (1) (2019) 307–315.

[57] E. Yun, J.H. Lee, J. Kim, H. Park, J. Lee, Identifying the nonradical mechanism in the peroxymonosulfate activation process: singlet oxygenation versus mediated electron transfer, Environ. Sci. Technol. 52 (12) (2018) 7032–7042.

[58] F.E. Scully, J. Hoigné, Rate constants for reactions of singlet oxygen with phenols and other compounds in water, Chemosphere 16 (4) (1987) 681–694.

[59] A.A. Frimer, The reaction of singlet oxygen with olefins: the question of mechanism, Chem. Rev. 79 (5) (1979) 359–387.

[60] D.R. Kearns, Physical and chemical properties of singlet molecular oxygen, Chem. Rev. 71 (4) (1971) 395–427.

[61] H. Li, Z. Zhao, J. Qian, B. Pan, Are free radicals the primary reactive species in Co (II)-mediated activation of peroxymonosulfate? New evidence for the role of the Co (II)-peroxymonosulfate complex, Environ. Sci. Technol. 55 (9) (2021) 6397–6406.

[62] J. Liang, X. Duan, X. Xu, K. Chen, Y. Zhang, L. Zhao, H. Qiu, S. Wang, X. Cao, Persulfate oxidation of sulfamethoxazole by magnetic iron-char composites via nonradical pathways: Fe(IV) versus surface-mediated electron transfer, Environ. Sci. Technol. 55 (14) (2021) 10077–10086.

[63] A. Jawad, K. Zhan, H. Wang, A. Shahzad, Z. Zeng, J. Wang, X. Zhou, H. Ullah, Z. Chen, Z. Chen, Tuning of persulfate activation from a free radical to a nonradical pathway through the incorporation of non-redox magnesium oxide, Environ. Sci. Technol. 54 (4) (2020) 2476–2488.

[64] S. Pang, J. Duan, Y. Zhou, Y. Gao, J. Jiang, Oxidation kinetics of anilines by aqueous permanganate and effects of manganese products: comparison to phenols, Chemosphere 235 (2019) 104–112.

[65] J. Yao, R. Qu, X. Wang, V.K. Sharma, A. Shad, A.A. Dar, Z. Wang, Visible light and fulvic acid assisted generation of Mn(III) to oxidize bisphenol A: the effect of tetrabromobisphenol A, Water Res. 169 (2020), 115273.

[66] L. Wang, J. Jiang, S. Pang, Y. Zhou, J. Li, S. Sun, Y. Gao, C. Jiang, Oxidation of bisphenol A by nonradical activation of peroxymonosulfate in the presence of amorphous manganese dioxide, Chem. Eng. J. 352 (2018) 1004–1013.

[67] Y. Jing, B.P. Chaplin, Mechanistic study of the validity of using hydroxyl radical probes to characterize electrochemical advanced oxidation processes, Environ. Sci. Technol. 51 (4) (2017) 2355–2365.

[68] K.D. Sugden, K.E. Wetterhahn, Reaction of chromium(V) with the EPR spin traps 5,5-dimethylpyrroline N-oxide and phenyl-N-tert-butylnitrone resulting in direct oxidation, Inorg. Chem. 35 (3) (1996) 651–657.

[69] L. Shen, Z. Chen, J. Kang, P. Yan, J. Shen, B. Wang, S. Zhao, L. Bi, S. Wang, Y. Cheng, N-nitrosodimethylamine formation during oxidation of N,N-dimethylhydrazine compounds by peroxymonosulfate: kinetics, reactive species, mechanism and influencing factors, J. Hazard. Mater. 428 (2022), 128191.

[70] L. Yang, Z. Chen, J. Shen, Z. Xu, H. Liang, J. Tian, Y. Ben, X. Zhai, W. Shi, G. Li, Reinvestigation of the nitrosamine-formation mechanism during ozonation, Environ. Sci. Technol. 43 (14) (2009) 5481–5487.